Mass Transfer in Magnetohydrodynamic Oscillatory Flow of Casson Liquid Through a Porous Horizontal Channel with Velocity Slip

Zaheer Abbas[1] , Muhammad Shakib Arslan[1*], Muhammad Yousuf Rafiq[1], Jafar Hasnain [2]

Abstract

Background: Casson liquid, a non-Newtonian fluid, exhibits unique rheological properties characterized by a yield stress below which it behaves as a solid, and above which it flows like a viscous fluid. These fluids show a shear-thinning behavior, where viscosity decreases with an increasing shear rate, making them relevant in various industrial and biological processes. Understanding the dynamics of Casson fluid flow under different conditions, such as in the presence of magnetic fields (MHD), permeable media, or chemical reactions, is essential for optimizing systems in fields ranging from biomedical applications to chemical engineering. Methods: This study investigates the mass transfer in magnetohydrodynamic oscillatory flow of a Casson liquid through a porous horizontal channel with velocity slip. The governing nonlinear partial differential equations were transformed into ordinary differential equations using similarity transformation. The exact solutions were obtained using Mathematica to analyze the effects of various physical parameters, including the Hartmann number, Schmidt number, wall expansion ratio, and slip parameter on flow dynamics. Results: The results indicate that an increase in the Reynolds number enhances velocity at the lower wall while reducing it at the upper wall. An increase in the wall expansion ratio leads to higher velocity at the center of the channel and lower velocity near the plate edges, modeling arterial dilation effects. The fluid parameter and slip parameter significantly influence velocity profiles, impacting flow dynamics relevant to biological and engineering applications. The Hartmann effect showed that velocity decreases at the channel center, demonstrating the importance of magnetic field strength in controlling fluid flow. Conclusion: This study offers insights into the behavior of Casson fluid flows in oscillating and porous environments, which are applicable to biomedical and industrial processes. The findings can be used to optimize cooling systems in electronic devices, enhance the design of medical devices, and improve treatments involving magnetic fields. Additionally, this insight can be applied in developing more efficient drug delivery systems that rely on the flow of therapeutic fluids through narrow channels or porous media.

Keywords: Casson liquid, Magnetohydrodynamics, Oscillatory flow, Porous channel, Velocity slip

Significance | This study demonstrated the understanding of Casson fluid dynamics under magnetic fields and slip conditions aids in optimizing cooling systems and enhancing biomedical applications.

*Correspondence. Muhammad Shakib Arslan, Department of Mathematics, The Islamia University of Bahawalpur, Bahawalpur 63100, Pakistan
E-mail: mshakibarslan12@gmail.com

Editor Md Nafiujjaman, Ph.D., And accepted by the Editorial Board Dec 02, 2022 (received for review Nov 01, 2022)

Introduction

Casson liquid, a non-Newtonian fluid, exhibits unique rheological performance described by a yield stress below which it behaves as a solid and above which it flows like a viscous fluid. Unlike Newtonian fluids, whose viscosity remains constant, Casson fluids

Author Affiliation.
[1] Department of Mathematics, The Islamia University of Bahawalpur, Bahawalpur 63100, Pakistan
[2]Department of Computer Science, Bahria University, Islamabad, Pakistan

Please cite this article:
Zaheer Abbas, Muhammad Shakib Arslan et al. (2022). Mass Transfer in Magnetohydrodynamic Oscillatory Flow of Casson Liquid Through a Porous Horizontal Channel with Velocity Slip, Biosensors and Nanotheranostics, 1(1), 1-13, 9823

demonstrate a shear-thinning property, where the viscosity declines with growing shear rate. This behavior makes Casson fluids particularly relevant in various industrial and biological processes where controlling flow and stress is critical, such as in the flow of blood, which is often modeled as a Casson fluid due to its viscoelastic properties (Casson, 1959). In engineering and scientific research, understanding the dynamics of Casson liquid flow under different conditions, such as in the presence of magnetic fields (MHD), permeable media, or chemical reactions, is essential for optimizing systems in fields ranging from biomedical applications to chemical engineering (Siddiqui & Mishra, 2007; Nadeem, Haq, & Lee, 2012; Mustafa, Hayat, Pop, & Hendi, 2012). The complexity of Casson fluid flow, particularly in the presence of additional factors like wall motion, slip conditions, and external forces, necessitates advanced mathematical modeling and numerical solutions to accurately predict and control the behavior of such fluids in practical applications (Venkatesan, Sankar, Hemalatha, & Yatim, 2013; Shehzad, Hayat, Qasim, & Asghar, 2013; Khalid, Khan, & Shafie, 2014; Bhattacharyya, Hayat, & Alsaedi, 2014; Hussanan, Salleh, Tahar, & Khan, 2014; Asma, Khan, Arshad, & Sharidan, 2015). Ramesh and Devakar (2015) analyzed Casson liquid movement with slip conditions through plates, concluding that an increase in the pressure gradient leads to a rise in liquid velocity and volumetric flow rate for both generalized Couette and Poiseuille flows. Varatharaj and Tamizharasi (2024) investigated the mixed convection thermalized flow of reactive magnetized Casson fluid over a permeable plate, while Abbas et al. (2024) explored heat transfer phenomena in thermalized magnetized Casson fluid flow over a plate.

Research into oscillatory fluid flow is crucial for its practical applications in marine environments, where the rhythmic variations of water movement due to ocean currents, tidal shifts, and waves are omnipresent. These studies are essential for understanding how such flows impact marine structures like pipelines, oil booms, and floating tunnels, which are subject to both constant and oscillatory forces. Analyzing the hydrodynamic responses of these structures, including water fragmentation and surface distortion, allows for the design of more resilient and efficient constructions. This knowledge is fundamental in enhancing the durability and safety of marine infrastructure against dynamic hydraulic conditions, providing critical insights for practical engineering challenges. Makinde and Mhone (2005) explored the effects of magnetohydrodynamics and radiative heat transfer on oscillatory flow in a porous channel. The effect of the Navier slip constraints on the hydromagnetic oscillatory flow of an incompressible viscous fluid in a planar channel that is also filled with a porous material was inspected by Mehmood and Ali (2007). An analytical solution for the two-dimensional oscillatory flow of an incompressible viscous fluid through a highly porous media confined by an infinite vertical plate was explored by Abdul-Hakeem and Sathiyanathan (2009). Furthermore, fascinating results on free convective oscillatory flows caused by time-dependent boundary conditions were published by Jha and Ajibade (2009, 2010, 2012). Umavathi, Chamkha, Mateen, and Al-Mudhaf (2009) inspected the heat transfer characteristics in the oscillatory flow of viscous liquid through a horizontal composite channel. Yuan and Wang (2019) conducted experiments in oscillatory tunnels to investigate the impact of acceleration skewness on the periodic vortex structure. They suggested that the presence of different vortices in two half periods contributes to the overall sediment transport. The precise characterization of vortex properties holds significant importance in understanding vortex dynamics. Earnshaw and Greated (1998) examined the periodic evolution of vortex center, radius, and strength on ripples under both oscillatory flow and waves, comparing their findings with those of a discrete vortex model. Malarkey and Davies (2002), and Chen and Yu (2015) employed similar methodologies to quantitatively analyze vortices, differing mainly in the definitions of vortex center, radius, and strength. The periodic vortex structure plays a crucial role in influencing the differences in boundary layer development and suspended sediment motion between ripples and flat bedforms. An experiment conducted to analyze the hydrodynamic forces acting on semi-submerged cylinders subjected to a combination of steady flow and oscillatory flow was investigated by Hu et al. (2023). The nonlinear behavior of oscillatory flow in a standing-wave thermoacoustic heat engine with high-pressure amplitude was investigated by Ja'fari and Jaworski (2023). A novel approach was employed to produce biodiesel from coconut waste cooking oil, utilizing a solar-powered rotating flask oscillatory flow reactor. The produced biodiesel was subsequently utilized in a diesel engine and was explored by Niyas and Shaji (2023). The heat transfer characteristics of magnetohydrodynamic two-fluid oscillatory flow in an inclined channel with a saturated porous medium were investigated by Bala Anasuya and Srinivas (2023).

The slip boundary condition is critical for understanding fluid interactions at solid interfaces, affecting flow dynamics in systems like microfluidic devices and nano-scale channels. It is essential for precise modeling in scenarios where fluid-solid interactions are crucial, such as thin fluid films. Addressing the complexity of these conditions, especially in compressible MHD systems, requires careful consideration of compatibility between nonlinear terms and slip conditions. Tang and Gao (2016) examined local strong solutions to the compressible MHD equations with an initial vacuum, where the velocity field adheres to the Navier-slip condition. Considering the fully compressible MHD system, Xi and Hao (2017) demonstrated the local existence of classical solutions to the initial-boundary value problem with slip boundary

conditions, excluding thermal conductivity, under certain initial data conditions. However, the global existence of strong (classical) solutions for general bounded smooth domains with initial vacuum density in the MHD system remains an open question. Recently, Cai and Li (2021) proved the global existence of classical solutions for the barotropic compressible Navier-Stokes equations in bounded domains with slip boundary conditions, despite the presence of vacuum and small energy, albeit possibly with large oscillations. They employed new techniques to obtain necessary a priori estimates, particularly boundary estimates, compared to previous works. Motivated by this research, Chen, Huang, and Shi (2021) investigated the initial-boundary-value problem of the isentropic compressible Navier-Stokes-Poisson equations in 3D bounded domains with slip boundary conditions and vacuum, considering large and non-flat doping profiles.

Based on the literature survey, the analysis of slip conditions and non-uniform wall concentrations on chemical reaction and mass transfer radiation in Casson liquid flows through a porous horizontal channel has not yet been reported. Therefore, we investigate the mass transfer in magnetohydrodynamic oscillatory flow of a Casson liquid through a porous horizontal channel with velocity slip. The governing nonlinear partial differential equations are transformed into ordinary differential equations using similarity transformation, and exact solutions are obtained using Mathematica. The effects of various physical parameters on flow variables are illustrated through graphs and tables. The findings offer practical applications for designing efficient cooling systems in electronic devices by optimizing velocity slip and wall temperature distribution to enhance heat transfer and improve device performance.

2. Problem Formulation

In this scenario, the flow of Casson fluid, a non-Newtonian fluid, is studied through a channel where the flow is unsteady and incompressible. The channel walls undergo time-dependent expansion and contraction, with non-uniform wall concentration influencing the flow dynamics. A perpendicular magnetic field is applied, impacting the fluid's velocity, while suction at the lower wall and blowing at the upper wall create a pressure differential driving the flow. However, it is assumed that the $x-$axis represents the direction of the fluid flow, while the $y-$axis is perpendicular to the plate. The fluid's concentration and velocity are influenced solely by the variables time t and y. This setup models complex fluid behaviors relevant to engineering, biological systems, and materials science.

The rheological equation for a Casson fluid, as defined by Raju and Sandeep [2]:

$$\tau_{ij}=\begin{cases}2e_{ij}\left(\mu_B+\frac{p_y}{\sqrt{2\pi}}\right), \pi>\pi_c,\\ 2\left(\mu_B+\frac{p_y}{\sqrt{2\pi}}\right)e_{ij}, \pi<\pi_c,\end{cases} \quad (1)$$

The problem equations can be defined based on the given assumptions

$$\frac{\partial v}{\partial y}+\frac{\partial u}{\partial x}=0, \quad (2)$$

$$\frac{\partial u}{\partial t}+v\frac{\partial u}{\partial y}+u\frac{\partial u}{\partial x}=-\frac{\partial p}{\partial x}\frac{1}{\rho}-\frac{\sigma_f B_0^2}{\rho}u+\nu\left(\frac{\partial^2 u}{\partial y^2}+\frac{\partial^2 u}{\partial x^2}\right)(1+1/\beta), \quad (3)$$

$$\frac{\partial v}{\partial t}+\frac{\partial v}{\partial y}v+u\frac{\partial v}{\partial x}=-\frac{\partial p}{\partial y}\frac{1}{\rho}+\nu\left(\frac{\partial^2 v}{\partial y^2}+\frac{\partial^2 v}{\partial x^2}\right)(1+1/\beta), \quad (4)$$

$$\frac{\partial C}{\partial t}+\frac{\partial C}{\partial y}v+u\frac{\partial C}{\partial x}=-k_1C+\left(\frac{\partial^2 C}{\partial y^2}+\frac{\partial^2 C}{\partial x^2}\right)D. \quad (5)$$

subjected to the boundary conditions

$$u=-\frac{\partial u}{\partial y}\frac{\sqrt{k_2}}{\sigma_1}, \quad v=-v_0=-\dot{a}A_0, \quad C=C_1, \text{ at } y=-a(t), \quad (6)$$

$$u=0, \quad v=-v_1=-\dot{a}A_1, \quad C=C_2, \text{ at } y=a(t), \quad (7)$$

Where t is time, $A_0=v_0/\dot{a}$ and $A_1=v_1/\dot{a}$ are the measure of porous permeability, B_0 denotes the magnetic field's strength, $\beta=\sqrt{\pi_c 2}\mu_B/P_y$ is the Casson parameter, C is the concertation field, ρ is the density, D is the mass diffusion, p is pressure, σ_f is the electric conductivity of the fluid, and k_1 is the reaction rate.

Applying a transformation to Eqs. (1) - (4) simplifies the equations, making them easier to solve or revealing deeper insights into the system's behavior. This approach enhances the manageability and interpretability of complex mathematical models.

$$\eta=\frac{y}{a}, \quad u=\frac{\nu x}{a^2}F'(\eta), \quad v=-\frac{\nu}{a}F(\eta), \quad (8)$$

Removing the pressure term simplifies the fluid dynamics equations by removing the influence of pressure changes, allowing for a more straightforward analysis focused on other forces affecting the flow. This approach results in a more manageable and analyzable set of equations.

$$F_{\eta\eta\eta\eta} - F_{\eta\eta}Mn - F_{\eta\eta}F_{\eta} + F_{\eta\eta\eta}F - a^2F_{\eta\eta t}v^{-1} + \alpha F_{\eta\eta\eta}\eta + 3F_{\eta\eta}\alpha = 0 \quad (9)$$

The wall expansion ratio a indicates the rate of wall movement, while the Hartmann number Mn measures the magnetic field's influence on fluid flow. Simplified boundary conditions reduce problem complexity, making the equations easier to solve.

$$F(1) = R, \quad F(-1) = R_0, \quad F'(-1) = F''(-1)\gamma, \quad F'(1) = 0, \quad (10)$$

After simplifying the momentum equation, we obtain the final form

$$\left(1+\frac{1}{\beta}\right)f^{iv} + ff''' \,\mathrm{Re} + 3f''\alpha - f''Mn + \eta\alpha f''' - \mathrm{Re}\, ff'' = 0 \quad (11)$$

Transformed boundary surfaces are adjusted to align with the transformed equations, ensuring consistency and solvability within the new mathematical framework.

$$f(-1) = A, \quad f(1) = 1, \quad f'(1) = 0, \quad f'(-1) = f''(-1)\gamma, \quad (12)$$

where $A = v_0 / v_1$.

The concentration of the liquid can be defined as:

$$C = \sum (x/a)^m C_m \phi_m(\eta) + C_1, \quad (13)$$

The upper wall concentration fluid can be expressed as:

$$C_2 = \sum (x/a)^m C_m \phi_m(\eta) + C_1, \quad (14)$$

After simplifying the concentration equation, we obtain the final form

$$\phi_m'' - \eta\phi_m'\alpha Sc - (-Sc\alpha Kr - 2m)\phi_m + \mathrm{Re}(\phi_m' f - f'\phi_m 2m)Sc = 0 \quad (15)$$

where $Sc = v/Da$ the Sherwood number and $Kr = K_1 v/\dot{a}$ the chemically reactions.

with the boundary surfaces:

$$\phi_m(-1) = 1, \quad \phi_m(1) = 0. \quad (16)$$

The surface friction coefficients C_f and Sherwood number Sh, which are stated as

$$C_f = \frac{t_w}{r_f n_w^2}, \qquad Sh = \frac{xj_w}{\mathrm{D}(C_1 - C_2)}, \quad (17)$$

where t_w is the skin friction and j_w is the mass flux from the surface, are defined as

$$t_w = m\left(\frac{\partial u}{\partial y}\right)_{y=0}, \qquad j_w = -D\left(\frac{\partial C}{\partial y}\right)_{y=0}, \quad (18)$$

using Eq. (17), we obtain

$$\mathrm{Re}^{1/2} C_f = |F''(0)|, \qquad Sh/\mathrm{Re}^{1/2} = |f\phi_m(0)|. \quad (19)$$

The boundary value problem described by Eqs. (11), and (15) is solved using an analytical approach via Mathematica. This analytical technique has been utilized in previous studies [31].

4. Results and discussion

The exact solutions for the governing equations (11) and (15), under the boundary conditions (12) and (16), are derived using the integration technique. The impact of key parameters, including the wall's Schmidt number, chemical reaction parameter, porosity parameter, fluid parameter, Hartmann number, slip parameter, and wall expansion ratio on velocity and concentration profiles, is analyzed through Figs. 2-14. The problem's validation is clearly presented in Table 1.

Fig. 2 demonstrates the impact of the Reynolds number on velocity, showing that an increase in the Reynolds number leads to higher velocity at the lower wall and a decrease at the upper wall. These results are consistent with previously reported findings, as depicted in the accompanying sketch. This insight is particularly useful in biological systems, where the Reynolds number is critical for understanding blood flow dynamics in vessels. An elevated Reynolds number at the lower wall, associated with higher shear stress, can improve nutrient delivery and waste removal at the vessel walls. Fig. 3 shows that increasing the wall expansion ratio leads to higher velocity at the center of the channel and lower velocity near the wider sections of the plate. In biological systems, this can model arterial dilation, where increased central flow promotes circulation, while reduced velocity near vessel walls may indicate areas of blood pooling or lower shear stress, potentially contributing to vascular conditions like atherosclerosis. Understanding these effects is crucial for developing targeted treatments for such conditions. Fig. 4 illustrates the effect of the fluid parameter on velocity, indicating that as the fluid parameter increases, velocity increases near the upper wall and decreases near the lower wall. The accompanying sketch also depicts the Newtonian effect. Understanding these dynamics is crucial for addressing conditions where blood viscosity is a factor, such as in clot formation or managing blood flow in patients with varying hematocrit levels. Fig. 5 illustrates the influence of the slip parameter on velocity, showing that an increase in the slip parameter results in higher velocity at the lower wall and

Box 1. **Nomenclature**

t'	Time	K	porous permeability
σ_e	electrical conductivity	B_0	intensity of the magnetic field
α	Walls expansion ratio	Mn	Hartmann's number
Kr	Chemical reaction parameter	Cf	skin friction
β	Casson parameter	C_1, C_2	concentration of the right and left wall
Si	Schmidt number	Nu	Nesselt number
u, v	velocity components		***Greek Symbols***
t	dimensional time	γ	slip velocity parameter
Pr	Prandtl number	ρ	fluid density
P	Pressure	μ	constant viscosity
C	concentration	k	thermal conductivity
(x, y)	Cartesian coordinate system	γ	cold wall slip parameters
Re	Reynold's number	σ	heated wall slip parameters
A	Permeability parameter	σ^*	Stefan-Boltzmann constant

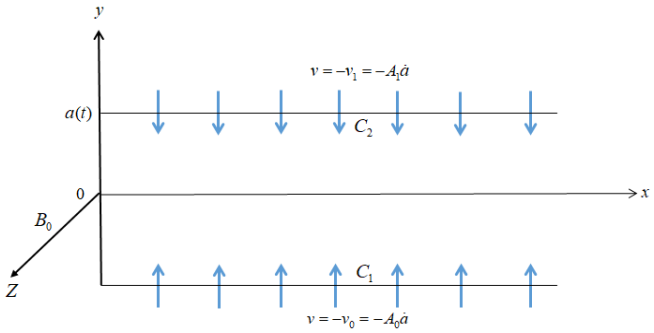

Figure 1. Flow geometry.

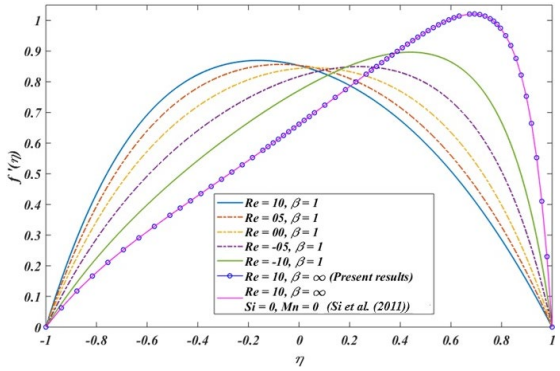

Figure 2. Influence of Re on $f'(\eta)$ solid line shows Xinhui [32] results and circle lines show present results when $\mathrm{Mn} = 1, A = -0.2,\ Kr = 2,\ \mathrm{Sc} = 1, Si = 0$ and $\alpha = -2$.

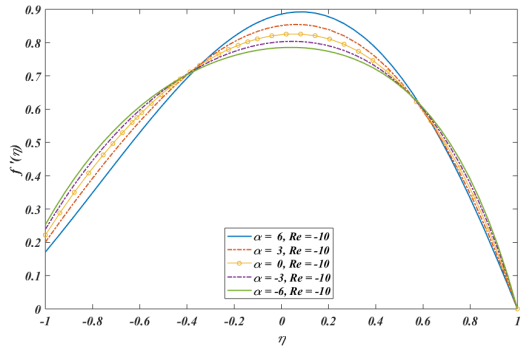

Figure 3. Impact of α 0n $f'(\eta)$ when $\mathrm{Mn}=1, A=-0.2,\ Kr=2, \mathrm{Sc}=1, Si=0.2$ and $\beta=0.5$.

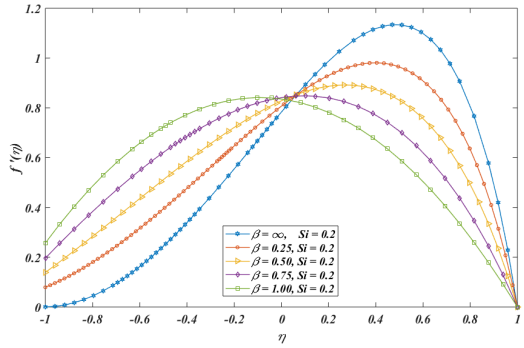

Figure 4. Impact of β 0n $f'(\eta)$ when $\mathrm{Mn}=1, A=-0.2,\ Kr=2, \mathrm{Sc}=1, \mathrm{Re}=-10$ and $\alpha=-2$.

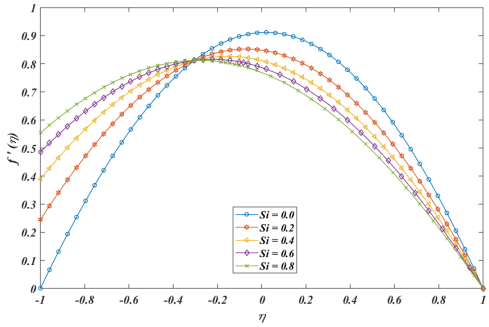

Figure 5. Impact of Si 0n $f'(\eta)$ when $\mathrm{Mn}=1, A=-0.2,\ Kr=2, \mathrm{Sc}=1, \mathrm{Re}=-10, \beta=0.5$ and $\alpha=-2$.

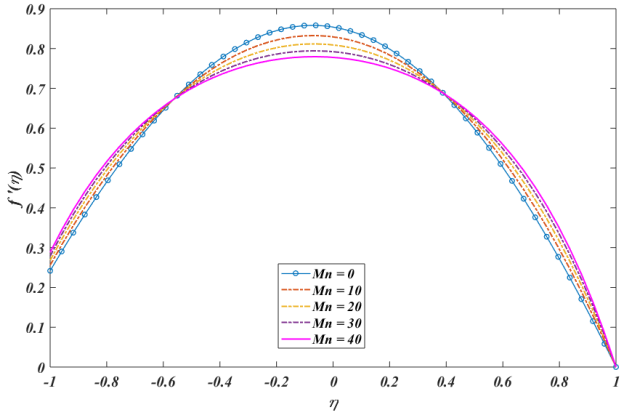

Figure. 6. Impact of Mn 0n $f'(\eta)$ when $Si=0.2, A=-0.2,\ Kr=2, \mathrm{Sc}=1, \mathrm{Re}=-10, \beta=0.5$ and $\alpha=-2$.

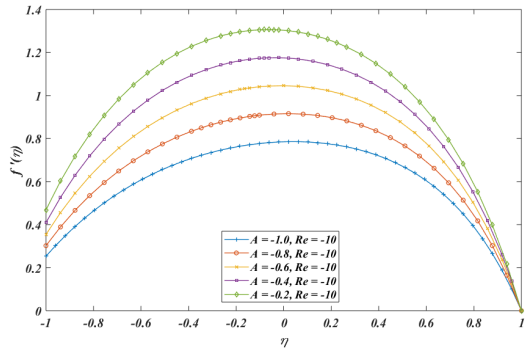

Figure 7. Impact of A 0n $f'(\eta)$ when $Si = 0.2, Mn = 1,\ Kr = 2, \mathrm{Sc} = 1, \mathrm{Re} = -10, \beta = 0.5$ and $\alpha = -2$.

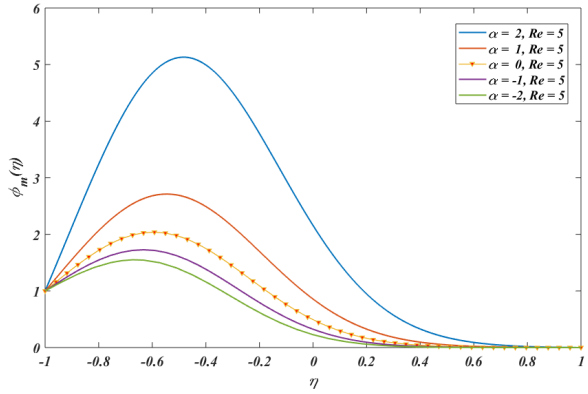

Figure 8. Impact of α 0n $\phi_m(\eta)$ when $Si = 0.2, Mn = 1,\ Kr = 2, \mathrm{Sc} = 1, A = -0.2$ and $\beta = 0.2$.

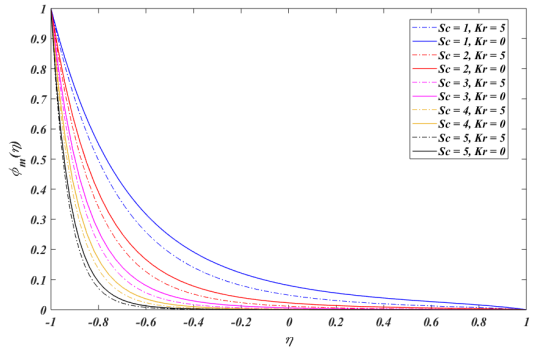

Figure 9. Impact of Sc and Kr 0n $\phi_m(\eta)$ when $Si = 0.2, Mn = 1,\ \beta = 0.2, \mathrm{Re} = -5, A = -0.2$ and $\alpha = -2$.

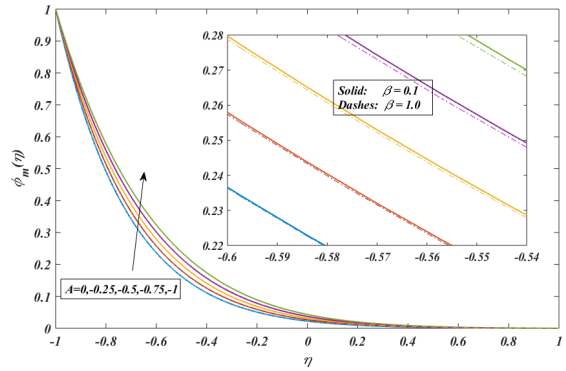

Figure 10. Impact of A 0n $\phi_m(\eta)$ when $Si = 0.2, Mn = 1,\ Kr = 2, \mathrm{Sc} = 1, A = -0.2, \mathrm{Re} = -5, \beta = 0.2$ and $\alpha = -2.$

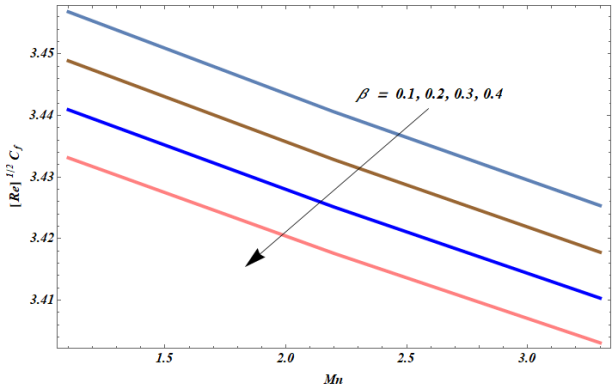

Figure 11. Impact of β 0n $\mathrm{Re}^{1/2} C_f$ when $Si = 0.2,\ Kr = 2, \mathrm{Sc} = 1, A = -0.2, \mathrm{Re} = 1$ and $\alpha = -2.$

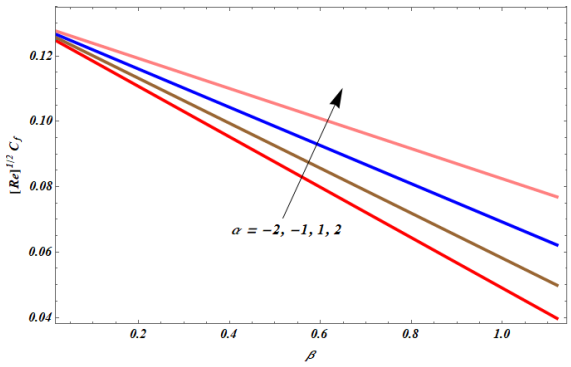

Figure 12. Impact of α 0n $\mathrm{Re}^{1/2} C_f$ when $Si = 0.2,\ Kr = 2, \mathrm{Sc} = 1, A = -0.2, \mathrm{Re} = 1$ and $\beta = -2.$

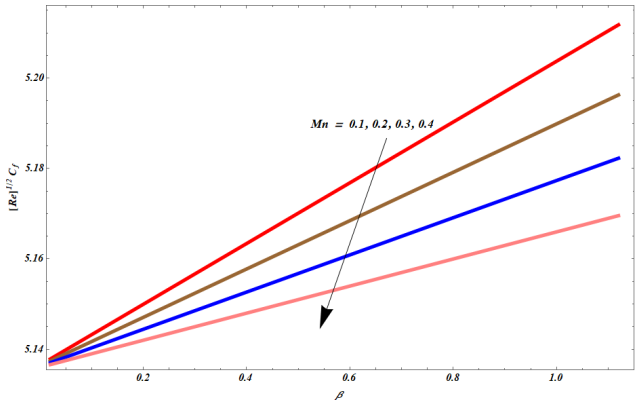

Figure 13. Impact of Mn 0n $\mathrm{Re}^{1/2} C_f$ when $Si = 0.2,\ Kr = 2, \mathrm{Sc} = 1, A = -0.2, \mathrm{Re} = 1$ and $\alpha = -2$.

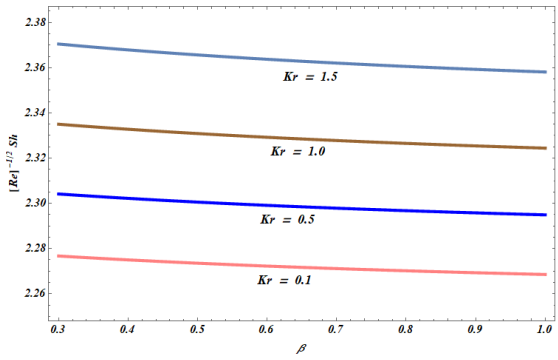

Figure 14. Impact of Kr 0n $\mathrm{Re}^{1/2} Sh$ when $Si = 0.2, Mn = 1,\ \mathrm{Sc} = 1, A = -0.2, \mathrm{Re} = 1$ and $\alpha = -2$.

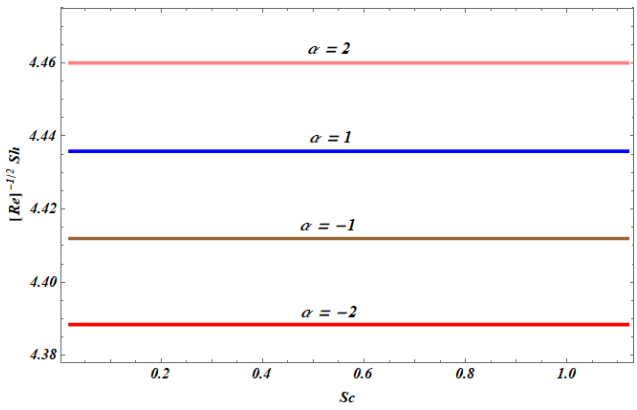

Figure 15. Impact of α 0n $\mathrm{Re}^{1/2} Sh$ when $Si = 0.2, Mn = 1,\ \mathrm{Sc} = 1, A = -0.2, \mathrm{Re} = 1$ and $Kr = 2$.

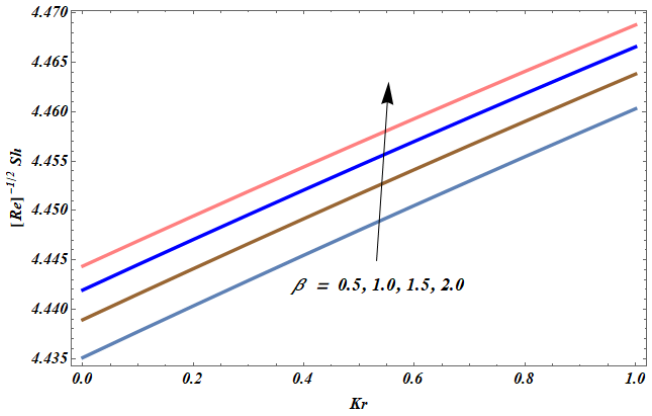

Figure 16. Impact of 0n $\mathrm{Re}^{1/2}\ Sh$ when $Si = 0.2, Mn = 1, \mathrm{Sc} = 1, A = -0.2, \mathrm{Re} = 1$ and $\alpha = -2.$

Table 1. Comparison of the current findings with previous literature.

α	η	Dogonchi et al. [34] results	Si et al. [33] results	Present results $Mn = 0,\ \beta = \infty$ and $Si = 0$
2	0.0	0.0	0.0	0.0
	0.2	1.250930	1.2515	1.2509300
	0.4	1.580277	0.58369	1.5802762
	0.6	1.283515	1.2824	1.283515
	0.8	0.683500	0.683691	0.683501
	1	0.0	0.0	0.0
6	0.0	0.0	0.0	0.0
	0.2	1.471667	1.47554	1.471665
	0.4	1.674527	0.67639	1.674527
	0.6	1.143492	1.14335	1.143492
	0.8	0.503774	0.502146	0.503774
	1	0.0	0.0	0.0

reduced velocity at the upper wall. Understanding this behavior is crucial for conditions like atherosclerosis, where changes in wall shear stress and blood flow dynamics can affect disease progression and influence treatment approaches. In Fig. 6, the Hartmann effect demonstrates that the velocity decreases at the center of the plate and increases near the walls due to the magnetic field's influence. This occurs because the Lorentz force dampens the fluid flow in the center while redistributing the velocity towards the walls. This effect is crucial in applications like MHD generators, nuclear reactor cooling systems, and medical devices where magnetic control of fluid flow is necessary. Fig. 7 shows the impact of the porosity parameter on velocity, indicating that velocity increases with a rise in porosity. This understanding is valuable for studying blood flow through porous structures like capillary networks or in engineered tissues, where optimizing porosity is essential for effective nutrient and oxygen delivery.

We observed from the Figs. 8-10 that the expansion ratio, Schmidt number, chemical reaction parameter, and porosity parameter significantly influence concentration, while other parameters are held constant. Fig. 8 shows that an increase in the expansion ratio leads to a rise in concentration within the flow. This occurs because the expanded space slows fluid velocity, allowing more time for substances to accumulate or react. This understanding is crucial in applications like chemical reactors, biological systems, and environmental engineering, where controlling concentration is important. Fig. 9 shows that increasing the Schmidt number raises concentration, while increasing the chemical reaction parameter reduces it. This understanding is vital for optimizing pollutant dispersion in environmental systems and enhancing drug delivery in biological systems, allowing for better control over concentration levels and improving the effectiveness of these processes. Fig. 10 shows that as the porosity parameter increases, concentration also rises. This occurs because higher porosity allows for greater fluid or substance movement through the medium, leading to increased accumulation. This understanding is crucial in applications like filtration, drug delivery, and soil management, where controlling fluid transport and distribution is essential.

Figs. 11-13 represents the variation of β, α, and Mn on $[\mathrm{Re}]^{1/2}C_f$. The impact of β against Mn is described in Fig. 11. It shows that $[\mathrm{Re}]^{1/2}C_f$ is an decreasing function of β. Similar effects are observed in Figure 12, which shows the impact of the wall expansion ratio on skin friction, indicating that skin friction increases as the wall expansion ratio rises. Conversely, Figure 13 illustrates the effect of the Hartmann number on skin friction, revealing that skin friction decreases as the Hartmann number increases. Figs. 14-16 are shown to describe the effects of Kr, α, and β on $[\mathrm{Re}]^{-1/2}Sh$. The Sherwood number increases with the rise in chemical reaction rate, wall expansion ratio, and Casson parameter.

5. Conclusion

In conclusion, Non-Newtonian fluids, including Casson fluids, play a crucial role in various biomedical and industrial applications such as cancer treatments, drug delivery, engine cooling, and heat exchangers. This study delves into the mass transfer phenomena associated with the hydromagnetic flow of Casson fluid through a horizontal porous channel, emphasizing the effects on skin friction and the Sherwood number. The analysis, supported by graphs and tables, demonstrates that increases in Reynolds number, Casson parameter, slip parameter, and Hartmann number lead to higher velocity and Sherwood number while reducing skin friction. Moreover, higher expansion ratio values enhance both velocity and concentration, and reduced porosity parameters further elevate velocity and mass concentration. Conversely, increasing Schmidt number and chemical reaction values decrease concentration and Sherwood number. The observed reduction in skin friction with rising Casson parameter is particularly pertinent for biomedical applications. Given that blood behaves similarly to Casson fluids, these findings can inform the design of medical devices such as stents and blood pumps, aiming to minimize frictional resistance and mitigate vessel damage. Additionally, the insights gained can enhance the development of efficient drug delivery systems, optimizing the flow of therapeutic fluids through narrow channels or porous media.

Author contributions

Z.A. and M.S.A. conceptualized the study. M.Y.R. contributed to data collection and analysis, while J.H. assisted with the manuscript drafting. All authors contributed to the final review and approved the manuscript.

Acknowledgment

The author would thankful to their department.

Competing financial interests

The authors have no conflict of interest.

References

Abbas, S., Parveen, I., Nisa, Z. U., Amjad, M., Metwally, A. S. M., Nazar, M., & Jan, A. Z. (2024). Effect of thermal radiation on fractional MHD Casson flow with the help of fractional operator. International Journal of Theoretical Physics, 63(8), 186. https://doi.org/10.1007/s10773-024-06047-2

Asma, K., Khan, I., Arshad, K., & Sharidan, S. (2015). Unsteady MHD free convection flow of Casson fluid past an oscillating vertical plate embedded in a porous medium.

Engineering Science and Technology, an International Journal, 18(2), 309-317. https://doi.org/10.1016/j.jestch.2015.02.004

Bala Anasuya, J., & Srinivas, S. (2023). Heat transfer characteristics of magnetohydrodynamic two-fluid oscillatory flow in an inclined channel with saturated porous medium. Proceedings of the Institution of Mechanical Engineers, Part C: Journal of Mechanical Engineering Science. https://doi.org/10.1177/09544089221146364

Bhattacharyya, K., Hayat, T., & Alsaedi, A. (2014). Exact solution for boundary layer flow of Casson fluid over a permeable stretching/shrinking sheet. ZAMM - Journal of Applied Mathematics and Mechanics/Zeitschrift Für Angewandte Mathematik Und Mechanik, 94(6), 522-528. https://doi.org/10.1002/zamm.201300106

Cai, G., & Li, J. (2021). Existence and exponential growth of global classical solutions to the compressible Navier-Stokes equations with slip boundary conditions in 3D bounded domains. arXiv preprint arXiv:2102.06348. https://doi.org/10.48550/arXiv.2102.06348

Casson, N. (1959). A flow equation for the pigment oil suspension of the printing ink type. In Rheology of Disperse Systems (pp. 84-102). Pergamon.

Chen, X., & Yu, X. (2015). A numerical study on oscillatory flow-induced sediment motion over vortex ripples. Journal of Physical Oceanography, 45(1), 228-246. https://doi.org/10.1175/JPO-D-14-00023.1

Chen, Y., Huang, B., & Shi, X. (2021). Global well-posedness of classical solutions to the compressible Navier-Stokes-Poisson equations with slip boundary conditions in 3D bounded domains. arXiv preprint arXiv:2102.07938. https://doi.org/10.48550/arXiv.2102.07938

Dogonchi, A. S., Alizadeh, M., & Ganji, D. D. (2017). Investigation of MHD Go-water nanofluid flow and heat transfer in a porous channel in the presence of thermal radiation effect. Advanced Powder Technology, 28(7), 1815-1825. https://doi.org/10.1016/j.apt.2017.04.001

Earnshaw, H. C., & Greated, C. A. (1998). Dynamics of ripple bed vortices. Experimental Fluid Mechanics, 25(3), 265-275. https://doi.org/10.1007/s003480050122

Hakeem, A. A., & Sathiyanathan, K. (2009). An analytic solution of an oscillatory flow through a porous medium with radiation effect. Nonlinear Analysis: Hybrid Systems, 3(3), 288-295. https://doi.org/10.1016/j.na-hs.2008.09.002

Hu, T., Ren, H., Shen, J., Niu, Z., Zhang, M., Xu, Y., ... & Sun, T. (2023). Experimental investigation on hydrodynamic forces of semi-submerged cylinders in combined steady flow and oscillatory flow. Ocean Engineering, 268, 113612. https://doi.org/10.1016/j.oceaneng.2023.113612

Hussanan, A., Salleh, M. Z., Tahar, R. M., & Khan, I. (2014). Unsteady boundary layer flow and heat transfer of a Casson fluid past an oscillating vertical plate with Newtonian heating. PLoS ONE, 9(10), e108763. https://doi.org/10.1371/journal.pone.0108763

Ja'fari, M., & Jaworski, A. J. (2023). On the nonlinear behavior of oscillatory flow in a high-pressure amplitude standing-wave thermoacoustic heat engine. International Journal of Heat and Mass Transfer, 201, 123595. https://doi.org/10.1016/j.ijheatmasstransfer.2023.123595

Jha, B. K., & Ajibade, A. O. (2009). Free convective flow of heat generating/absorbing fluid between vertical porous plates with periodic heat input. International Communications in Heat and Mass Transfer, 36(6), 624-631. https://doi.org/10.1016/j.icheatmasstransfer.2009.01.015

Jha, B. K., & Ajibade, A. O. (2010). Free convective flow between vertical porous plates with periodic heat input. ZAMM - Journal of Applied Mathematics and Mechanics/Zeitschrift Für Angewandte Mathematik Und Mechanik, 90(3), 185-193. https://doi.org/10.1002/zamm.200810217

Jha, B. K., & Ajibade, A. O. (2012). Effect of viscous dissipation on natural convection flow between vertical parallel plates with time-periodic boundary conditions. Communications in Nonlinear Science and Numerical Simulation, 17(4), 1576-1587. https://doi.org/10.1016/j.cnsns.2011.07.029

Khalid, A., Khan, I., & Shafie, S. (2014). Exact solutions for unsteady free convection flow of Casson fluid over an oscillating vertical plate with constant wall temperature. Abstract and Applied Analysis, 2014, Article ID 946350. https://doi.org/10.1155/2014/946350

Makinde, O. D., & Mhone, P. Y. (2005). Heat transfer to MHD oscillatory flow in a channel filled with porous medium. Romanian Journal of Physics, 50(9/10), 931-938. https://doi.org/10.5550/RJF-50-9-10-2005-01

Malarkey, J., & Davies, A. G. (2002). Discrete vortex modeling of oscillatory flow over ripples. Applied Ocean Research, 24(3), 127-145. https://doi.org/10.1016/S0141-1187(02)00014-8

Mehmood, A., & Ali, A. (2007). The effect of slip condition on unsteady MHD oscillatory flow of a viscous fluid in a planar channel. Romanian Journal of Physics, 52(1/2), 85-94. https://doi.org/10.5550/RJF-52-1-2-2007-01

Mustafa, M., Hayat, T., Pop, I., & Hendi, A. A. (2012). Stagnation-point flow and heat transfer of a Casson fluid towards a stretching sheet. Z. Naturforsch, 67(1-2), 70-76. https://doi.org/10.5560/ZNA.2012-0007

Nadeem, S., Haq, R. U., & Lee, C. (2012). MHD flow of a Casson fluid over an exponentially shrinking sheet. Scientia Iranica, 19(6), 1550-1553. https://doi.org/10.1016/j.scient.2012.04.004

Niyas, M. M., & Shaija, A. (2023). Biodiesel production from coconut waste cooking oil using a novel solar-powered rotating flask oscillatory flow reactor and its utilization in a diesel engine. Thermal Science and Engineering Progress, 40, 101794. https://doi.org/10.1016/j.tsep.2023.101794

Ramesh, K., & Devakar, M. (2015). Some analytical solutions for flows of Casson fluid with slip boundary conditions. Ain Shams Engineering Journal, 6(4), 967-975. https://doi.org/10.1016/j.asej.2014.09.003

Shehzad, S. A., Hayat, T., Qasim, M., & Asghar, S. (2013). Effects of mass transfer on MHD flow of Casson fluid with chemical reaction and suction. Brazilian Journal of Chemical Engineering, 30(1), 187-195. https://doi.org/10.1590/S0104-66322013000100018

Si, X. H., Zheng, L. C., Zhang, X. X., & Chao, Y. (2011). Homotopy analysis solutions for the asymmetric laminar flow in a porous channel with expanding or contracting walls. Acta Mechanica Sinica, 27(2), 208-214. https://doi.org/10.1007/s10409-011-0053-7

Siddiqui, S. U., & Mishra, S. (2007). A study of modified Casson's fluid in modeled normal and stenotic capillary-tissue diffusion phenomena. Applied Mathematics and Computation, 189(2), 1048-1057. https://doi.org/10.1016/j.amc.2007.01.061

Tang, T., & Gao, H. (2016). Strong solutions to 3D compressible magnetohydrodynamic equations with Navier-slip condition. Mathematical Methods in the Applied Sciences, 39(10), 2768-2782. https://doi.org/10.1002/mma.3666

Umavathi, J. C., Chamkha, A. J., Mateen, A., & Al-Mudhaf, A. (2009). Unsteady oscillatory flow and heat transfer in a horizontal composite porous medium channel. Nonlinear Analysis: Model and Control, 14(3), 397-415. https://doi.org/10.15388/NA.2009.14.3.26

Varatharaj, K., & Tamizharasi, R. (2024). Multiple solution of MHD Casson fluid flow in porous channel with chemical reactions and thermal radiation effects. Journal of Magnetism and Magnetic Materials, 172205. https://doi.org/10.1016/j.jmmm.2023.172205

Venkatesan, J., Sankar, D. S., Hemalatha, K., & Yatim, Y. (2013). Mathematical analysis of Casson fluid model for blood rheology in stenosed narrow arteries. Journal of Applied Mathematics, 583-809. https://doi.org/10.1155/2013/583809

Xi, S., & Hao, X. (2017). Existence of the compressible magnetohydrodynamic equations with vacuum. Journal of Mathematical Analysis and Applications, 453(1), 410-433. https://doi.org/10.1016/j.jmaa.2017.03.011

Yuan, J., & Wang, D. (2019). An experimental investigation of acceleration-skewed oscillatory flow over vortex ripples. Journal of Geophysical Research: Oceans, 124(12), 9620-9643. https://doi.org/10.1029/2019JC015309